

Controllable Polarization and Diffraction Modulated Multi-Functionality Based on Metasurface

Ruizhe Zhao, Guangzhou Geng, Qunshuo Wei, Yue Liu, Hongqiang Zhou, Xue Zhang, Cong He, Xin Li, Xiaowei Li, Yongtian Wang, Junjie Li,* and Lingling Huang*

Diffraction gratings are crucial optical elements in various optical systems, which can realize tailored diffraction energy distributions as well as phase modulations based on Fourier series. Meanwhile, the polarization gratings can produce arbitrarily specified polarization states on a set of desired diffraction orders for realizing polarimeter. However, simultaneously and independently tailoring the encoded phase profiles and polarization states in different diffraction orders has not been investigated previously. Here, a dielectric metasurface with the capability of generating different holographic images (generalized phase profiles) in different diffraction orders with controllable polarization states is proposed. Such functionality is achieved by applying the double-phase method into the metasurface design process for manipulating the complex amplitude distributions of two orthogonal polarization bases. Furthermore, in order to prove that the proposed design strategy is suitable to achieve complicated wavefront modulation in a straightforward and convenient manner, a vectorial holographic image with spatially continuous polarization distribution is also obtained without any iteration process. The proposed method may pave the way to achieve a variety of applications such as beam shaping, polarization imaging as well as multifunctional optical systems.

for arbitrarily tailoring the fundamental properties of light such as amplitude,^[1,2] phase,^[3–5] polarization,^[6–8] frequency^[9,10] as well as simultaneous multiple parameters modulation^[11–14] with high resolution. Therefore, a wide range of novel applications has been successfully demonstrated including beam shaping,^[15,16] metalens,^[17–19] holography,^[20–22] nonlinear optics,^[23,24] and color printing^[25,26] with the assistance of versatile wavefront modulation methods provided by metasurfaces.

For clearly investigating the wavefront modulation of output light, the Jones matrix method is commonly adopted to link the relation between the output light and input light. Meanwhile, achieving arbitrary Jones matrix by elaborately designed metasurfaces is in favor of many meaningful applications. By analyzing the eigenvalue and eigenvector of desired Jones matrix at each pixel, dielectric metasurfaces with the capability of controlling the phase and polarization of output

light simultaneously have been successfully demonstrated, leading to enormous polarization multiplexing schemes.^[11,27–29] Combining singular value decomposition with double-phase method, arbitrary symmetric Jones matrix can be realized using unitary platforms.^[30] The proposed method was utilized to achieve desired propagation-dependent polarization response and dramatically decrease the complexity of the required optical system compared to traditional methods. Furthermore, several polarization functionalities that can only be achieved with high degrees of freedom (DOFs) of the Jones matrix have been successfully demonstrated based on coherent pixel method.^[31] Hence, the diverse design freedoms offered by meta-atoms for realizing desired Jones matrix as well as a variety of smart algorithms can motivate metasurfaces to achieve many novel functionalities that may not be easily accomplished in traditional optics.

Diffraction gratings are crucial optical elements for imaging, optical communication, spectrometer, polarization measurement, and many other applications. For example, in order to achieve orbital angular momentum (OAM) multiplexing communication, the vortex gratings are utilized to generate multiple vortex beams with controllable topological charges in different diffraction orders based on Fourier series.^[32,33] Moreover, different phase functions can be integrated with Damman grating concept for generating arrays of beams including vortex


1. Introduction

The ultrathin metasurfaces composed of plasmonic or dielectric nanoantennas have gradually become practical platforms

R. Zhao, Q. Wei, Y. Liu, H. Zhou, X. Zhang, C. He, X. Li, Y. Wang, L. Huang
Beijing Engineering Research Center of Mixed Reality and Advanced Display
School of Optics and Photonics
Beijing Institute of Technology
Beijing 100081, China
E-mail: huanglingling@bit.edu.cn

G. Geng, J. Li
Beijing National Laboratory for Condensed Matter Physics
Institute of Physics
Chinese Academy of Sciences
Beijing 100191, China
E-mail: jjli@iphy.ac.cn

X. Li
Laser Micro/Nano-Fabrication Laboratory
School of Mechanical Engineering
Beijing Institute of Technology
Beijing 100081, China

 The ORCID identification number(s) for the author(s) of this article can be found under <https://doi.org/10.1002/adom.202102596>.

DOI: 10.1002/adom.202102596

beams, bessel beams as well as airy beams arrays.^[34–38] While, the polarization states of each diffraction order in above-mentioned methods are usually consistent and cannot be tailored arbitrarily. In order to achieve polarization states generation and measurement, metasurface has been applied through optimizing the phase distributions within the supercell to obtain the desired Fourier coefficients of each diffraction order.^[39] Such method can be extended from 1D polarization grating to a 2D version for controlling the polarization responses of different diffraction orders based on a birefringence dielectric metasurface. Meanwhile, a compact full-Stokes parallel snapshot polarization camera was successfully demonstrated for achieving polarization imaging without moving parts.^[40] Although the polarization states of different diffraction orders can be tailored arbitrarily based on above-mentioned methods, the phase profiles encoded in different orders are set uniform in the design process.

Here, we propose a novel method for encoding generalized phase profiles into different diffraction orders with controllable polarization states. A dielectric metasurface that can reconstruct different holographic images in different diffraction orders with distinct vectorial features is demonstrated by manipulating the complex amplitude distributions based on the double-phase method without spatial multiplexing. Furthermore, we generate a vectorial holographic image with spatially continuous polarization distribution without any iteration process for proving that our proposed design strategy is suitable to achieve complicated wavefront modulation. Hence, we reveal the simultaneously and independently tailoring the phase,

polarization, and diffraction orders that have not been investigated yet. The proposed method may pave the way to achieve a variety of applications including beam shaping, polarization imaging as well as multifunctional optical systems.

2. Results

A schematic illustration of the proposed dielectric metasurface for encoding generalized phase profiles into different diffraction orders and manipulating the corresponding polarization states simultaneously is shown in **Figure 1**. The demonstrated metasurface is designed based on double-phase method according to the desired complex amplitude distributions $T_{h,x}$ and $T_{h,y}$. When a 45° linearly polarized light illuminating on the metasurface, the complex amplitude distributions of two orthogonal polarization bases T_{xx} and T_{yy} can be arbitrarily controlled. And the output light can lead the reconstruction of different holographic images (the number “1”, “2”, “3”, and “4” are chosen as the original images) in different diffraction orders with controllable polarization states (0°, 30°, 60°, and 90° linearly polarized states) without multiplexing schemes. This novel functionality can be contributed to the complex amplitude modulation of two orthogonal polarization bases T_{xx} and T_{yy} provided by the dielectric metasurface which may be difficult to be accomplished by utilizing the spatial light modulator (SLM) in traditional optics.

Before designing our demonstrated dielectric metasurface, we need to analyze the principle of vortex grating at first. For

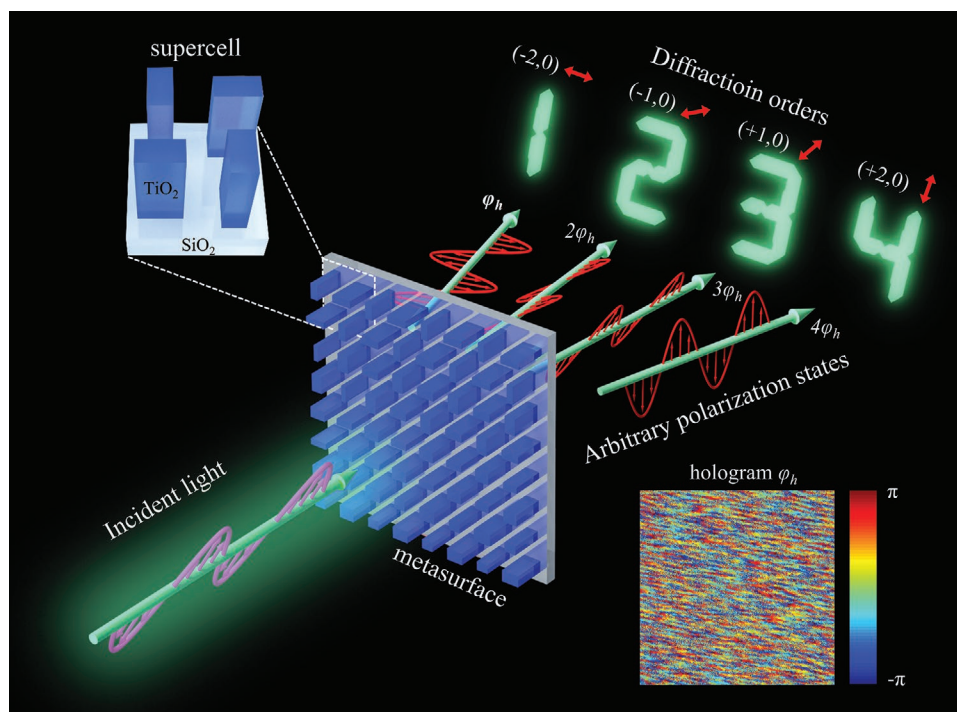


Figure 1. Schematic illustration of our designed dielectric metasurface. The demonstrated metasurface can encode generalized phase profiles into different diffraction orders with controllable polarization states. The numbers “1”, “2”, “3”, and “4” are chosen as the original images. The pink arrow indicates the polarization state of incident light is 45° linearly polarized. Meanwhile, the red arrows represent the polarization state of each diffraction order. The hologram ϕ_h that is utilized to realize the desired metasurface is shown in the bottom right corner.

a traditional 1D vortex grating in x -direction, its transmission function can be expressed by Fourier series:

$$T_{VG-x} = \sum_{m=-\infty}^{\infty} c_{mx} \exp(iml_x \varphi) \exp\left(im \frac{2\pi}{D_x} x\right) \quad (1)$$

where c_{mx} is the Fourier coefficient for the m th diffraction order, l_x is the intrinsic base topological charge in x direction, φ represents the azimuthal angle, and D_x indicates the period of the grating. The Fourier coefficient c_{mx} is an important property of vortex gratings which can determine the intensity and polarization state of different diffraction orders. In general, the c_{mx} can be tailored by optimizing the phase profiles in each period. With the assistance of several optimized approaches such as genetic algorithm, simulated annealing algorithm, and gradient descent optimization, the optimized phase profile is acquired in order to improve the efficiency and performance of the demonstrated vortex grating.^[36] By encoding the optimized phase profile into a SLM or T_{xx} channel of designed metasurface, a row of optical vortices in x direction with different topological charges can be realized but with consistent polarization states.

Inspired by the realization of 1D vortex grating, we propose a strategy to encode generalized phase profiles into different diffraction orders with controllable polarization states based on dielectric metasurface. First, a hologram φ_h that is analogous to the azimuthal angle distribution φ in 1D vortex grating is optimized through the gradient descent method.^[41] While for the diffraction order $m = -2, -1, 1, \text{ and } 2$, we have phase profile of $\varphi_h, 2\varphi_h, 3\varphi_h, \text{ and } 4\varphi_h$. The flowchart of the optimization is shown in **Figure 2**. A random phase profile φ_h composed of 550×550 pixels is generated for the initialization. The intensity in the hologram plane is set as uniform distribution I_0 in each iteration. The Fourier transform (FFT) is utilized to realize the propagation process from the hologram plane to the object plane. We adopt the mean squared error (MSE) to evaluate the difference between the reconstructed image and original image. By

calculating the gradient $\nabla_{\varphi_h} e_t(\varphi_h)$ that is the derivative of the total error $e_t \left(e_t = \sum_{d=1}^4 e_d \right)$ to the phase profile φ_h , the updated φ_h can be generated in each iteration. In the optimization process, we have to find a phase profile φ_h that can minimize the total error e_t . After a sufficient number of iterations (500 times), we obtain the optimized hologram φ_h that enable us to reconstruct different holographic images in k -space with satisfied image qualities based on the phase profiles $\varphi_h, 2\varphi_h, 3\varphi_h, \text{ and } 4\varphi_h$, where the multiplier factors 1, 2, 3, and 4 are encoded to achieve independent modulation. The entire optimization takes nearly 600 s in a personal computer (CPU: Intel i7 11700KF, RAM: 32GB).

Then, we calculate two complex amplitude distributions T_{h-x} and T_{h-y} which need to be encoded in T_{xx} and T_{yy} polarization basis according to Equation (2):

$$\begin{cases} T_{h-x} = \sum_{m \in \{q\}} c_{mx} \exp(in\varphi_h) \exp\left(im \frac{2\pi}{D_x} x\right) \\ T_{h-y} = \sum_{m \in \{q\}} c_{my} \exp(in\varphi_h) \exp\left(im \frac{2\pi}{D_x} x\right) \end{cases} \quad (2)$$

where the diffraction order m is set as $-2, -1, +1, \text{ and } +2$ in the process of designing the demonstrated metasurface. Meanwhile, an integer $n = 1, 2, 3, \text{ and } 4$ is multiplied by the hologram φ_h in different diffraction orders corresponding to the above holographic flowchart, respectively. The period of the grating D_x is set as $4.2 \mu\text{m}$. The Fourier coefficients in Equation (2) can be represented in the form of Jones vector $[c_{mx}, c_{my}]^T$ and are chosen as linearly polarized light with different polarization angle ($[1, 0]^T, [\cos(\pi/3), \sin(\pi/3)]^T, [\cos(2\pi/3), \sin(2\pi/3)]^T, \text{ and } [0, 1]^T$) for the convenience of experimental demonstration. Other polarization states including circular polarization state and elliptical polarization state are also achievable in our scheme (more details are provided in Section B of the

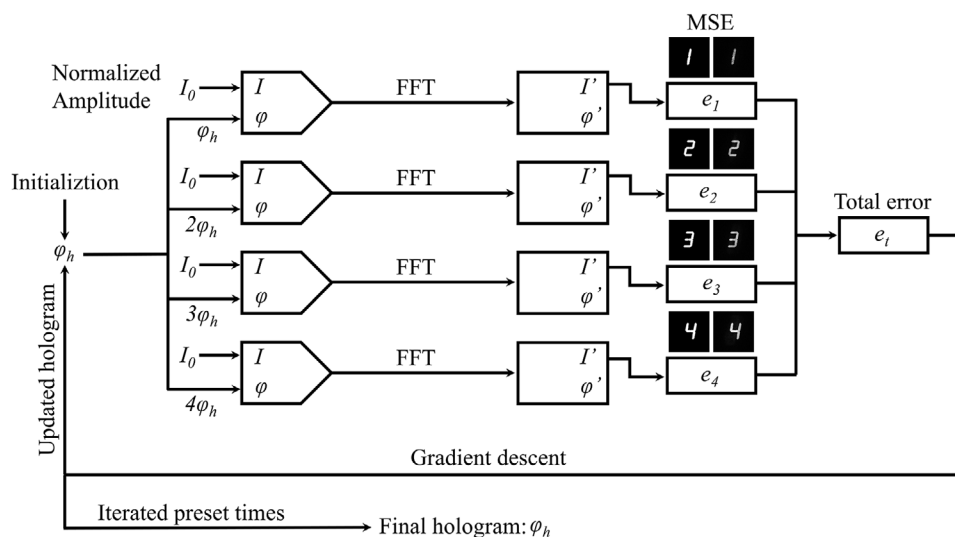


Figure 2. The flowchart of the optimization method for generating the hologram. The “FFT” represents the Fourier transform for investigating the propagation processes from hologram plane to the object plane. The errors of different diffraction orders ($e_1, e_2, e_3, \text{ and } e_4$) are calculated by mean squared error (MSE) method in order to evaluate the difference between the reconstructed images and target images. The total error is represented by e_t .

Supporting Information). Due to the difficulty in simultaneously and completely manipulating the complex amplitude of the c_{mx} and c_{my} based on phase only modulation, we choose a complex amplitude modulation approach instead. The calculated complex amplitude distributions T_{h_x} and T_{h_y} after normalization are encoded into the two orthogonal polarization basis T_{xx} and T_{yy} of the designed metasurface by utilizing the double-phase method. In this manner, the Fourier coefficients c_{mx} and c_{my} that determine the polarization states of different diffraction orders can be directly controlled by the proposed method.

The relation between the output (E^{out}) and input light (E^{in}) is commonly linked based on Jones matrix method and can be expressed in linear polarization basis as follows:

$$E^{\text{out}} = TE^{\text{in}} \text{ where } T = \begin{bmatrix} T_{xx} & T_{xy} \\ T_{yx} & T_{yy} \end{bmatrix} \quad (3)$$

The subscript i and j of the polarization channel T_{ij} indicate the output and input polarization components, respectively. By applying the double-phase method to the metasurface design process, an arbitrary Jones matrix T with $T_{xy} = T_{yx} = 0$ can be decomposed into the sum of two unitary matrices T_1 and T_2 as follows:^[30,42]

$$T = \begin{bmatrix} a_{xx}e^{i\varphi_{xx}} & 0 \\ 0 & a_{yy}e^{i\varphi_{yy}} \end{bmatrix} = \frac{1}{2} \begin{bmatrix} e^{i\varphi_{xx}^1} & 0 \\ 0 & e^{i\varphi_{yy}^1} \end{bmatrix} + \frac{1}{2} \begin{bmatrix} e^{i\varphi_{xx}^2} & 0 \\ 0 & e^{i\varphi_{yy}^2} \end{bmatrix} \quad (4)$$

where the phase items in T_1 and T_2 are calculated by $\varphi_{ii}^1 = \varphi_{ii} + \cos^{-1}(a_{ii})$ and $\varphi_{ii}^2 = \varphi_{ii} - \cos^{-1}(a_{ii})$ ($ii = xx$ or yy). In order to fulfill the unitary matrices T_1 and T_2 , a TiO₂ nanofin on top of a quartz substrate is chosen as the sub-unit of our demonstrated metasurfaces. As known, the high-index dielectric

nanofin can be considered as a tiny waveguide with different effective refractive index (n_{eff}) along its long and short axis which exhibits form birefringence. By tailoring the size of the nanofin, arbitrary phase shifts can be imposed on the orthogonal polarization components of output light and realize the matrix T_1 or T_2 . For covering the phase shifts from 0 to 2π with high efficiency and avoiding the coupling effect of neighbor sub-units, the period P and height H of the TiO₂ nanofin in each sub-unit are chosen as 350 and 600 nm, respectively. The amplitude ($\text{abs}(t_{xx})$ and $\text{abs}(t_{yy})$) and phase (φ_x and φ_y) of the transmission coefficients t_{xx} and t_{yy} are calculated by using rigorous coupled wave analysis (RCWA) method (more details are provided in Section A of the Supporting Information). Our demonstrated metasurfaces are composed of the supercell shown in Figure 3a. In each supercell, the 2×2 nanofins with different sizes are utilized to encode the desired complex amplitude distributions to the metasurface. Meanwhile, the sizes of the nanofins in diagonal and anti-diagonal positions are determined according to Equation (4) by guaranteeing the minimum of the error $\varepsilon = \text{abs}(t_{xx} - \exp(i\varphi_{xx}^i)) + \text{abs}(t_{yy} - \exp(i\varphi_{yy}^i))$ ($ii = 1, 2$) at each pixel. Therefore, the normalized T_{h_x} and T_{h_y} can be successfully encoded.

Then, we fabricated two types of metasurfaces named sample 1 and sample 2 on top of a fused quartz substrate by electron beam lithography for experimental demonstration (detail information is provided in Section D of the Supporting Information). The corresponding scanning electron microscopy images of sample 1 with a top view and side view are shown in Figure 3b,c. Our fabricated metasurfaces composed of 550×550 supercells with the period $2P = 700$ nm. Each supercell contained 2×2 TiO₂ nanofins with different sizes (L_1, L_2, W_1, W_2 ; 60–260 nm, $H = 600$ nm) but fixed orientation angles θ ($\theta = 0^\circ$).

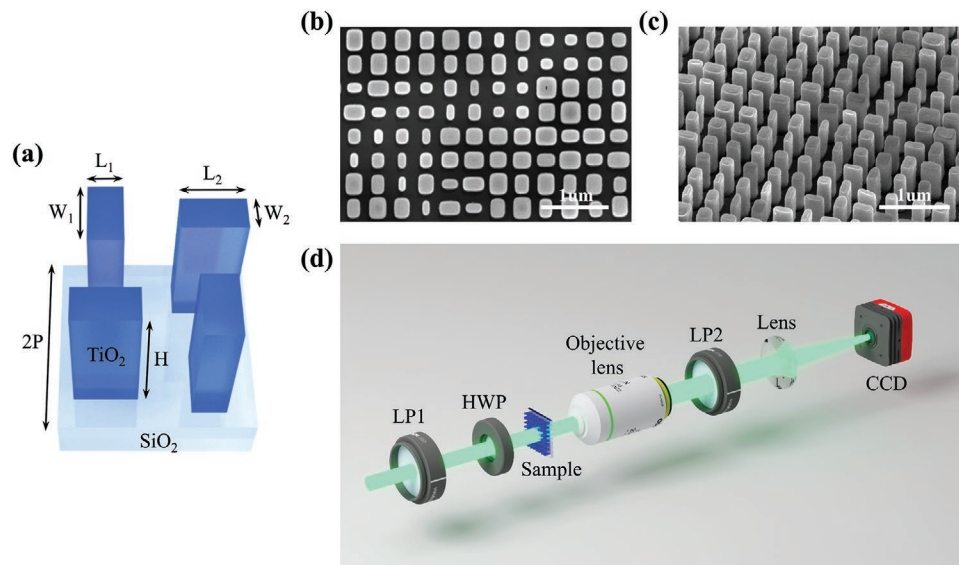


Figure 3. a) Schematic illustration of the supercell (2×2 TiO₂ nanofins) of metasurfaces. b,c) The scanning electron microscopy images of our fabricated metasurface sample 1 in top and side view. The metasurface are composed of 550×550 supercells. d) The experimental setup for capturing the holographic images in different diffraction orders. A linear polarizer LP1 and a half-wave plate HWP are used to control the polarization of incident light. Another linear polarizer LP2 is used as an analyzer to distinguish the polarization states in different diffraction orders. The fabricated metasurface sample is placed on the focal plane of an objective lens ($40\times/0.55$). A CCD camera is placed at the back focal plane of a lens ($f = 100$ mm) in order to capture the reconstructed images in k -space.

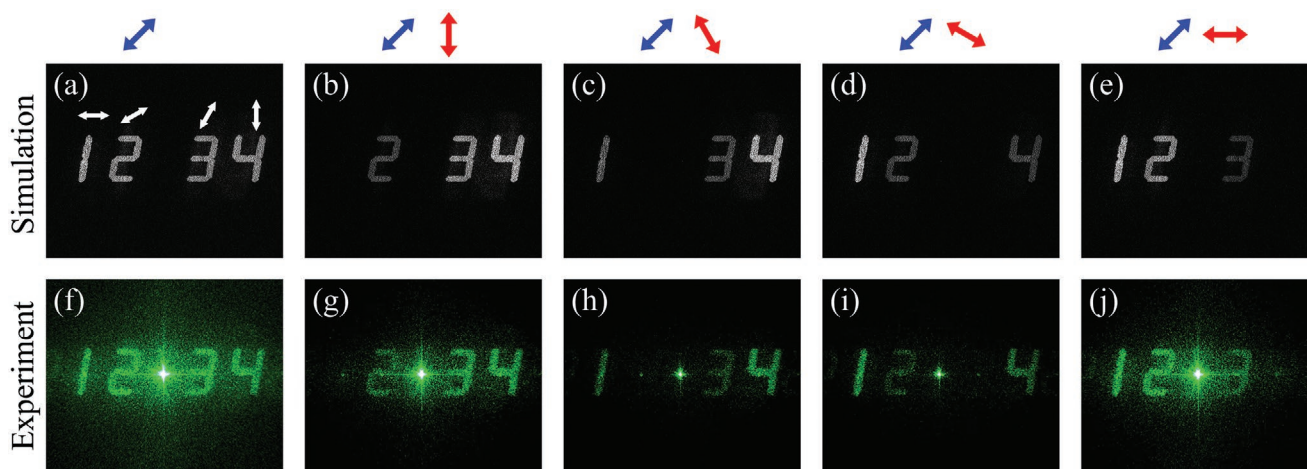


Figure 4. a–j) Simulated and experimental results of our fabricated metasurface sample 1 for reconstructing different holographic images in different diffraction orders with controllable polarization states. The wavelength of incident light is 532 nm. The blue and red arrows indicate the polarization of input and output light.

The simulated and experimental results of sample 1 are provided in **Figure 4**. When the 45° linearly polarized with the wavelength of 532 nm illuminating on the fabricated metasurface, the holographic images “1”, “2”, “3”, and “4” encoded in different diffraction orders are successfully obtained as depicted in **Figure 4f**. In order to discriminate the inconsistent polarization states of the four holographic images, we rotate the transmission axis of LP2 to different directions ($\theta_0 = 90^\circ, 120^\circ, 150^\circ, \text{ and } 180^\circ$) sequentially. The correct extinct phenomena are clearly observed as shown in **Figure 4g–j** that agree well with the corresponding simulated results. Meanwhile, we can find that four bright spots appear in the middle of each holographic images. These results can prove that the four holographic images with inconsistent polarization states are realized from the perspective of diffractive grating instead of the method for achieving vectorial holography. The designed diffraction angles of different diffraction order ($m = -2, -1, +1, \text{ and } +2$) that are calculated by Equation (2) are $-14.67^\circ, -7.28^\circ, 7.28^\circ, \text{ and } 14.67^\circ$, respectively. And the NA of the objective lens used in our experiment is 0.55, which is adequate to collect all the desired holographic images. In addition, our demonstrated method is quite different from other strategies which can accomplish the similar functionality in a multiplexing scheme.^[43–45] In the experiment, the measured transmission efficiency of the sample 1 is 46.7%. And the diffraction efficiency that is defined as the power of the reconstruct holographic images (observed without LP2) divided by the power of the incident light is 9.34%. The relative low efficiency of our demonstrated metasurface is mainly caused by the complex amplitude modulation of our proposed method as well as the existence of high order diffraction orders due to the pixel size $2P$ is slightly larger than the wavelength of incident light (more details are provided in Supporting Information).

Furthermore, a vectorial holographic image is also obtained without any iteration process in order to demonstrate the complicated wavefront modulation and can be realized in a straightforward and convenient manner. We select a picture of a rabbit as the original image. The rabbit is designed to

possess a spatially continuous polarization distribution as shown in **Figure 5a**. From left to right part of the rabbit, the corresponding polarization state is gradually changed from x -linear polarization state to y -linear polarization state as depicted by the black arrows. For an arbitrary polarization state $|\lambda\rangle$, it can be expressed by the Jones vector $|\lambda\rangle = [\cos \chi, e^{i\delta} \sin \chi]^T$ ($-\pi \leq \chi \leq \pi, -\pi \leq \delta = \delta_y - \delta_x \leq \pi$) in linear polarization basis. The polarization states are determined by the parameter χ and δ , but the phases (δ_x and δ_y) of x - and y -polarization component (E_{vx}, E_{vy}) of the electric field at the object plane are the design freedoms we can utilize. Due to the polarization distribution of the rabbit that is composed of linear polarization states with different orientation angles, the phase shifts δ is set to zero at each pixel. In **Figure 5b**, the process of generating the desired complex amplitude distributions E_{mx} and E_{my} is illustrated. The polarization components E_{vx} and E_{vy} at the object plane can be calculated as follows:

$$\begin{cases} E_{vx} = A_i \cos \chi e^{i\delta_i} \\ E_{vy} = A_i \sin \chi e^{i\delta_i} \end{cases} \quad (5)$$

where A_i indicates the amplitude distribution of the original image (a rabbit) and δ_i is a random phase profile. Then, the desired complex amplitude distribution E_{mx} and E_{my} at the hologram plane can be obtained by the inverse Fourier transform (IFFT) and encoded into the metasurface based on our proposed method. In addition, the random phase profile δ_i is necessary for avoiding the pixels with high amplitude values that are all accumulated in the center of the metasurface. The experimental and simulated results of the vectorial holographic image are shown in **Figure 5c–l**. A rabbit image with uniform intensity is successfully acquired and agrees well with the simulated result. The spatially continuous polarization distribution is verified by rotating the transmission axis of analyzer LP2 across different direction. The correct extinct phenomena shown in **Figure 5i–l** prove that our proposed method can realize the reconstruction of a vectorial holographic image (arbitrary polarization distribution) without any iteration process.

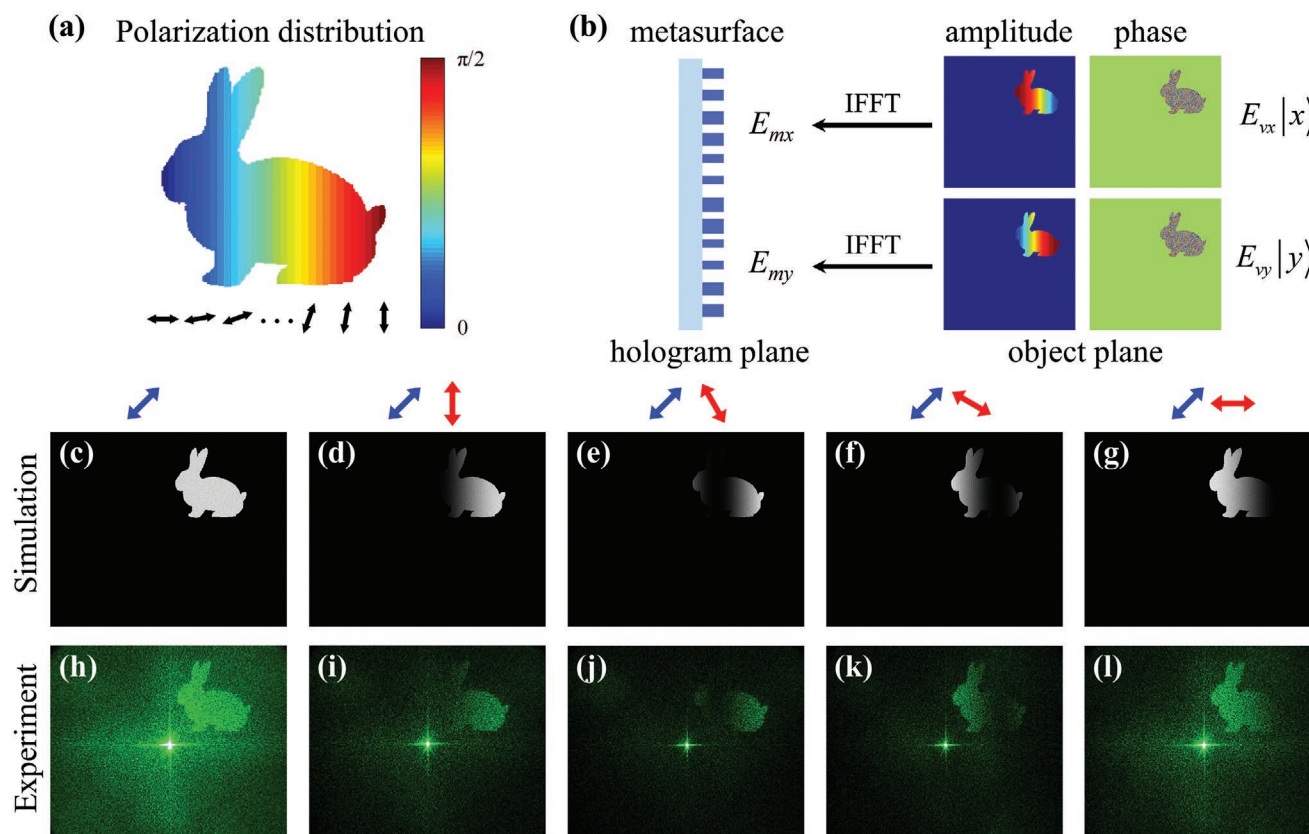


Figure 5. a) The polarization distribution of the original image (a rabbit) that is designed as linear polarization states with different orientation angles. b) The illustration of the process of generating the desired complex amplitude distributions E_{mx} and E_{my} . c–l) Simulated and experimental results of the vectorial holography based on sample 2. The blue and red arrows indicate the polarization of input and output light. Correct extinct phenomena can be observed by rotating the analyzer LP2.

3. Discussion

The mechanism of complex amplitude modulation lead to the relative low efficiencies of our fabricated metasurfaces. This may be improved by manipulating the Fourier coefficients c_{mx} and c_{my} with advanced optimized algorithms or deep learning method. Then, the functionality proposed here may be accomplish based on a phase-only platform with higher efficiency. Meanwhile, the quantified phase relations that acquired from the optimization are not necessary. Arbitrary and independent phase profiles can also be encoded into different diffraction orders with tailored polarization states (more details are provided in Section B of the Supporting Information). Because the optical functionalities including light focusing or vortex beam generation are all wavefront modulation which can be realized by encoding desired phase profiles to the metasurface. Therefore, simultaneously realizing different optical functionalities in different diffraction orders is achievable by our proposed design strategy. Furthermore, the broadband properties of the sample 1 and 2 are also provided in Figure S4 of the Supporting Information.

In summary, we have demonstrated a novel method for encoding generalized phase profiles into different diffraction orders with controllable polarization states. Different holographic images are successfully encoded into different diffraction orders with distinct vectorial features. This is achieved by manipulating the complex amplitude distributions of two orthogonal

polarization channels T_{xx} and T_{yy} based on double-phase method. Furthermore, a vectorial holographic image with spatially continuous polarization distribution is realized without any iteration process by utilizing the proposed design strategy. The proposed method here may pave the way to achieve a variety of applications such as beam shaping, polarization imaging and detection, optical tweezers as well as multifunctional optical systems.

4. Experimental Section

The experimental setup used in the experiment are shown in Figure 3d. Light from a supercontinuum laser source (NKT Photonics Super EVO) was passed through a linear polarizer LP1 and a half-wave plate HWP. The LP1 and HWP were used together to generate the 45° linearly polarized light illuminating on the metasurfaces. The fabricated metasurface samples were placed at the working distance of an objective lens ($40\times/\text{NA} = 0.55$). A charge coupled device camera (CCD) was placed at the back focal plane of a lens ($f = 100$ mm) in order to capture the reconstructed holographic images in k -space. And another linear polarizer LP2 was used as an analyzer to discriminate the polarization states of the reconstructed images that were encoded in different orders.

Supporting Information

Supporting Information is available from the Wiley Online Library or from the author.

Acknowledgements

The authors acknowledge the funding provided by the National Key R&D Program of China (2021YFA1401200), Beijing Outstanding Young Scientist Program (BJJWZYJH01201910007022), National Natural Science Foundation of China (No. U21A20140, No. 92050117) program, Fok Ying-Tong Education Foundation of China (No.161009) and Beijing Municipal Science&Technology Commission, Administrative Commission of Zhongguancun Science Park (No. Z211100004821009).

Author Contributions

R.Z. and G.G. contributed equally to this work. L.H. proposed the idea, R.Z. conducted pattern designs and numerical simulations, R.Z., Q.W., Y.L., Q.Z., X.Z., and C.H. conducted the hologram generations, G.G. and J.L. fabricated the samples, R.Z. performed the measurements, R.Z. and L.H. prepared the manuscript. L.H. and Y.W. supervised the overall projects. All the authors analyzed the data and discussed the results.

Conflict of Interest

The authors declare no conflict of interest.

Data Availability Statement

The data that support the findings of this study are available from the corresponding author upon reasonable request.

Keywords

complex amplitude modulation, diffraction modulation, metasurfaces, vectorial holography

Received: November 30, 2021

Revised: January 5, 2022

Published online:

- [1] K. Huang, H. Liu, F. J. Garcia-Vidal, M. Hong, B. Luk'yanchuk, J. Teng, C.-W. Qiu, *Nat. Commun.* **2015**, 6, 7059.
- [2] J. Li, Y. Zhang, J. Li, X. Yan, L. Liang, Z. Zhang, J. Huang, J. Li, Y. Yang, J. Yao, *Nanoscale* **2019**, 11, 5746.
- [3] N. Yu, P. Genevet, M. A. Kats, F. Aieta, J.-P. Tetienne, F. Capasso, Z. Gaburro, *Science* **2011**, 334, 333.
- [4] S. Sun, Q. He, S. Xiao, Q. Xu, X. Li, L. Zhou, *Nat. Mater.* **2012**, 11, 426.
- [5] L. Huang, X. Chen, H. Mühlenbernd, G. Li, B. Bai, Q. Tan, G. Jin, T. Zentgraf, S. Zhang, *Nano Lett.* **2012**, 12, 5750.
- [6] F. Aieta, P. Genevet, M. A. Kats, N. Yu, R. Blanchard, Z. Gaburro, F. Capasso, *Nano Lett.* **2012**, 12, 4932.
- [7] S. Kruk, B. Hopkins, I. I. Kravchenko, A. Miroshnichenko, D. N. Neshev, Y. S. Kivshar, *APL Photonics* **2016**, 1, 030801.
- [8] T. Li, L. Huang, J. Liu, Y. Wang, T. Zentgraf, *Opt. Express* **2017**, 25, 4216.
- [9] G. Li, S. Chen, N. Pholchai, B. Reineke, P. W. H. Wong, E. Y. B. Pun, K. W. Cheah, T. Zentgraf, S. Zhang, *Nat. Mater.* **2015**, 14, 607.
- [10] W. Ye, F. Zeuner, X. Li, B. Reineke, S. He, C.-W. Qiu, J. Liu, Y. Wang, S. Zhang, T. Zentgraf, *Nat. Commun.* **2016**, 7, 11930.
- [11] A. Arbabi, Y. Horie, M. Bagheri, A. Faraon, *Nat. Nanotechnol.* **2015**, 10, 937.
- [12] A. C. Overvig, S. Shrestha, S. C. Malek, M. Lu, A. Stein, C. Zheng, N. Yu, *Light: Sci. Appl.* **2019**, 8, 92.
- [13] Z. L. Deng, M. Jin, X. Ye, S. Wang, T. Shi, J. Deng, N. Mao, Y. Cao, B. O. Guan, A. Alù, *Adv. Funct. Mater.* **2020**, 30, 1910610.
- [14] Y. Bao, J. Ni, C. W. Qiu, *Adv. Mater.* **2020**, 32, 1905659.
- [15] W. T. Chen, M. Khorasaninejad, A. Y. Zhu, J. Oh, R. C. Devlin, A. Zaidi, F. Capasso, *Light: Sci. Appl.* **2017**, 6, e16259.
- [16] F. Yue, D. Wen, J. Xin, B. D. Gerardot, J. Li, X. Chen, *ACS Photonics* **2016**, 3, 1558.
- [17] M. Khorasaninejad, W. T. Chen, R. C. Devlin, J. Oh, A. Y. Zhu, F. Capasso, *Science* **2016**, 352, 1190.
- [18] W. T. Chen, A. Y. Zhu, V. Sanjeev, M. Khorasaninejad, Z. Shi, E. Lee, F. Capasso, *Nat. Nanotechnol.* **2018**, 13, 220.
- [19] S. Wang, P. C. Wu, V.-C. Su, Y.-C. Lai, M.-K. Chen, H. Y. Kuo, B. H. Chen, Y. H. Chen, T.-T. Huang, J.-H. Wang, *Nat. Nanotechnol.* **2018**, 13, 227.
- [20] L. Huang, X. Chen, H. Mühlenbernd, H. Zhang, S. Chen, B. Bai, Q. Tan, G. Jin, K.-W. Cheah, C.-W. Qiu, *Nat. Commun.* **2013**, 4, 2808.
- [21] G. Zheng, H. Mühlenbernd, M. Kenney, G. Li, T. Zentgraf, S. Zhang, *Nat. Nanotechnol.* **2015**, 10, 308.
- [22] R. Zhao, L. Huang, Y. Wang, *Photonix* **2020**, 1, 20.
- [23] L. Wang, S. Kruk, K. Koshelev, I. Kravchenko, B. Luther-Davies, Y. Kivshar, *Nano Lett.* **2018**, 18, 3978.
- [24] G. Hu, X. Hong, K. Wang, J. Wu, H.-X. Xu, W. Zhao, W. Liu, S. Zhang, F. Garcia-Vidal, B. Wang, *Nat. Photonics* **2019**, 13, 467.
- [25] X. Duan, S. Kamin, N. Liu, *Nat. Commun.* **2017**, 8, 14606.
- [26] Q. Wei, B. Sain, Y. Wang, B. Reineke, X. Li, L. Huang, T. Zentgraf, *Nano Lett.* **2019**, 19, 8964.
- [27] J. B. Mueller, N. A. Rubin, R. C. Devlin, B. Groever, F. Capasso, *Phys. Rev. Lett.* **2017**, 118, 113901.
- [28] R. C. Devlin, A. Ambrosio, N. A. Rubin, J. B. Mueller, F. Capasso, *Science* **2017**, 358, 896.
- [29] R. Zhao, B. Sain, Q. Wei, C. Tang, X. Li, T. Weiss, L. Huang, Y. Wang, T. Zentgraf, *Light: Sci. Appl.* **2018**, 7, 95.
- [30] A. H. Dorrah, N. A. Rubin, A. Zaidi, M. Tamagnone, F. Capasso, *Nat. Photonics* **2021**, 15, 287.
- [31] Y. Bao, L. Wen, Q. Chen, C.-W. Qiu, B. Li, *Sci. Adv.* **2021**, 7, eabh0365.
- [32] T. Lei, M. Zhang, Y. Li, P. Jia, G. N. Liu, X. Xu, Z. Li, C. Min, J. Lin, C. Yu, *Light: Sci. Appl.* **2015**, 4, e257.
- [33] H. Tan, J. Deng, R. Zhao, X. Wu, G. Li, L. Huang, J. Liu, X. Cai, *Laser Photonics Rev.* **2019**, 13, 1800278.
- [34] I. Moreno, J. A. Davis, B. M. L. Pascoguin, M. J. Mitry, D. M. Cottrell, *Opt. Lett.* **2009**, 34, 2927.
- [35] I. Moreno, J. A. Davis, D. M. Cottrell, N. Zhang, X.-C. Yuan, *Opt. Lett.* **2010**, 35, 1536.
- [36] L. Huang, X. Song, B. Reineke, T. Li, X. Li, J. Liu, S. Zhang, Y. Wang, T. Zentgraf, *ACS Photonics* **2017**, 4, 338.
- [37] Z. Lin, X. Li, R. Zhao, X. Song, Y. Wang, L. Huang, *Nanophotonics* **2019**, 8, 1079.
- [38] S. Lei, X. Zhang, S. Zhu, G. Geng, X. Li, J. Li, Y. Wang, X. Li, L. Huang, *Opt. Express* **2021**, 29, 18781.
- [39] N. A. Rubin, A. Zaidi, M. Juhl, R. P. Li, J. B. Mueller, R. C. Devlin, K. Leósson, F. Capasso, *Opt. Express* **2018**, 26, 21455.
- [40] N. A. Rubin, G. D'Aversa, P. Chevalier, Z. Shi, W. T. Chen, F. Capasso, *Science* **2019**, 365, eaax1839.
- [41] P. Georgi, Q. Wei, B. Sain, C. Schlickriede, Y. Wang, L. Huang, T. Zentgraf, *Sci. Adv.* **2021**, 7, eabf9718.
- [42] O. Mendoza-Yero, G. Mínguez-Vega, J. Lancis, *Opt. Lett.* **2014**, 39, 1740.
- [43] Q. Song, A. Baroni, R. Sawant, P. Ni, V. Brandli, S. Chenot, S. Vézian, B. Damilano, P. de Mierry, S. Khadir, *Nat. Commun.* **2020**, 11, 2651.
- [44] I. Kim, J. Jang, G. Kim, J. Lee, T. Badloe, J. Mun, J. Rho, *Nat. Commun.* **2021**, 12, 3614.
- [45] R. Zhao, X. Xiao, G. Geng, X. Li, J. Li, X. Li, Y. Wang, L. Huang, *Adv. Funct. Mater.* **2021**, 31, 2100406.